Title	Ultraviolet f→f emission and crystal field analysis for Er3+ in Cs2NaErCl6
Author(s)	Tanner, PA; Mak, CSK; Kwok, WM; Phillips, DL; Faucher, MD
Citation	Physical Review B - Condensed Matter And Materials Physics, 2002, v. 66 n. 16, p. 1652031-16520313
Issued Date	2002
URL	http://hdl.handle.net/10722/42634
Rights	Physical Review B (Condensed Matter and Materials Physics). Copyright © American Physical Society.

Ultraviolet $f \rightarrow f$ emission and crystal field analysis for Er^{3+} in $Cs_2NaErCl_6$

P. A. Tanner and C. S. K. Mak
Department of Biology and Chemistry, City University of Hong Kong, Tat Chee Avenue, Kowloon, Hong Kong SAR, People's Republic of China

W.-M. Kwok and D. L. Phillips
Department of Chemistry, The University of Hong Kong, Pokfulam Road, Hong Kong SAR, People's Republic of China

Michèle D. Faucher
UMR 8580 du CNRS, "Structures, Proprietes et Modelisation des Solides," Ecole Centrale Paris, 92295 Châtenay-Malabry Cedex, France

(Received 24 September 2001; revised manuscript received 21 May 2002; published 3 October 2002)

Luminescence is reported from the $^2I_{11/2}$ level of Er^{3+}, in the cubic elpasolite lattices $Cs_2NaErCl_6$ and Cs_2NaYCl_6. Altogether, with the use of ultraviolet laser excitation, 11 transitions from $^2I_{11/2}$ Γ_7 (at 40 668 cm^{-1}) to lower term multiplets have been observed and assigned. Transitions are also reported from the $^2K_{13/2}$ Γ_6 level at 32 613 cm^{-1}. The absence of emission from $^2P_{3/2}$ (at 31 367 cm^{-1}) under the experimental conditions is rationalized. Up-conversion to $^2H(2)_{9/2}$, which is not due to two-photon absorption, is reported for $Cs_2NaErCl_6$ under blue pulsed laser excitation. Trap emission from $^2G_{9/2}$ defect sites has been observed under ultraviolet excitation. A preliminary investigation has been made of the electronic absorption spectra of $Cs_2NaErCl_6$ and 58 Kramers quartet and doublet levels have been assigned, with a further 18 levels uncertain. The energy-level fit to 58 levels with total degeneracy 180 has been performed with a mean deviation of 20.4 cm^{-1}, which is improved to 16.8 cm^{-1} if an empirical correction to the diagonal reduced matrix element of U^4 for the $^2H(2)$ term is included. The average error is similar for the 18 uncertain levels (total degeneracy 52). A comparison is included with the energy-level parametrizations of other Er^{3+} systems.

DOI: 10.1103/PhysRevB.66.165203 PACS number(s): 71.70.Ch, 78.40.−q, 78.55.−m

I. INTRODUCTION

Recently, Dieke's diagram has been extended into the vacuum ultraviolet for several lanthanide ions from the results of excitation spectra using synchrotron radiation.[1] We are investigating the ultraviolet emission spectra of lanthanide ions from previously uncharacterized levels,[2,3] using anti-Stokes H_2-shifted frequency-tripled Nd-YAG excitation. In this study we report, and interpret in detail, the luminescence spectra from 40 700 to 11 000 cm^{-1} of Er^{3+} in the cubic elpasolite lattice,[4] and identify a previously unreported luminescent state. Classic studies of selective excitation and decay of Er^{3+} emission in LaF_3,[5] and energy-transfer phenomena in $CaF_2:Er^{3+}$,[6] have shown a wealth of luminescent states of Er^{3+} in crystals. In particular, the luminescence properties of Er^{3+} in the *elpasolite* lattice $Cs_2NaLnCl_6$ are unique due to the long lifetimes of excited states.[7,8] Up-conversion from the infrared to visible[9–11] and from the visible to ultraviolet[8,12–15] have been studied and the decay kinetics were investigated in detail. The effects of nonradiative processes upon several emission transitions of Er^{3+} in the elpasolite lattice have been investigated, and down-conversion cross-relaxation processes, involving one Er^{3+} initially in the electronic ground state, were found to be important in heavily Er^{3+}-doped crystals.[16,17] More generally, several previous studies have concerned the absorption and excitation spectra,[18,19] the emission spectra,[8] and the vibronic intensities[20,21] of $Cs_2NaErCl_6$, in addition to the energy-level parametrizations.[22,23]

In this work, the experimental details are briefly reviewed in Sec. II, and a summary of the results from the absorption spectrum of $Cs_2NaErCl_6$ is given in Sec. III A. Sections III B–III G comprise the major results from luminescence spectroscopy. Energy-level calculations utilizing the new data set are presented in Sec. IV A, and are compared with previous energy-level parametrizations in Sec. IV B. A summary of the main conclusions is made in Sec. V.

II. EXPERIMENT

$Cs_2NaErCl_6$ and $Cs_2NaYCl_6:Er^{3+}$ were prepared in polycrystalline form according to Morss method E.[4,19] Absorption spectra were recorded using a Biorad FTS-60A spectrometer with an external deuterium lamp source. The deuterium lamp was also employed with an Acton 0.5-m monochromator, having a 1800 g mm^{-1} grating blazed at 250 nm, and a back-illuminated SpectruMM charge coupled device (CCD). The latter spectra were not background corrected, and although the resolution was adequate, they serve as survey spectra since weak bands are not distinguished from noise in many cases. The sample was housed in an Oxford Instruments closed cycle cooler cryostat, with a base temperature of 10 K. Emission spectra were recorded using a tunable Panther OPO system pumped by the third harmonic of a Surelite Nd-YAG pulsed laser. Calibrations were made to vacuum wave numbers using a low-pressure mercury lamp. Emission spectra were also recorded at 10 K using the anti-Stokes hydrogen-shifted harmonics of frequency-tripled radiation from a Nd-YAG pulsed laser. The emission was collected at 90° and passed through an Acton 0.5-m spec-

TABLE I. Vibrational data for $Cs_2NaErCl_6$ at 10–20 K.

Normal mode of $ErCl_6^{3-a}$	Unit-cell group mode[a,b]	Raman spectrum (cm^{-1})	Components in vibronic spectra (cm^{-1})[c]
ν_1, α_{1g}, Er-Cl sym. str.	S_1	298	
ν_2, ε_g, Er-Cl sym. str.	S_2	236	
	S_3 τ_{1g} rot.		
	S_5 Cs^+ str.	47	45
ν_3, τ_{1u}, Er-Cl asym. str.	S_6		245, 259, 286
ν_4, τ_{1u}, Cl-Er-Cl b.	S_7		109, 116, 132
ν_5, τ_{2g}, Cl-Er-Cl b.	S_4	126	
	S_8 Na str.		182
	S_9 Cs^+ transl.		58, 69
ν_6, τ_{2u}, Cl-Er-Cl b.	S_{10}		78, 84

[a]Sym. is symmetric; str. is stretch; asym. is antisymmetric; b. is bend; rot. is rotatory mode; trans. is translatory mode.
[b]Reference 26.
[c]The features comprise contributions not only from $\mathbf{k}=0$.

trometer with a liquid-nitrogen-cooled SDS 9000 CCD. In all experiments the spectral resolution was between 2 and 4 cm^{-1}.

III. RESULTS AND DISCUSSION

$Cs_2NaErCl_6$ crystallizes in the space group $Fm3m$ and retains this structure at liquid-helium temperature.[24] The Er^{3+} ion in the $ErCl_6^{3-}$ moiety has O_h site symmetry. Vibrational data are available for gerade modes from low-temperature Raman spectra,[25] and for ungerade modes from the vibronic sidebands of the optical spectra at low temperature.[8,19] The latter spectra show dispersion and transverse-longitudinal mode splittings so that a multiple structure is observed for each internal moiety mode. Table I summarizes this, and includes the energies of the unit-cell group modes due to Na^+ and Cs^+ motions also.

Our starting point, for the energy-level assignments, is summarized in Fig. 1. This shows the energy levels of Er^{3+}, as calculated from the previous 18-parameter model, in which seven parameters were varied.[23] The energy levels in Fig. 1 are labeled by the dominant state, and some cases the *SLJ* parentage is mixed (e.g., for $^4G_{7/2}$ near 28 000 cm^{-1}, the leading eigenvector comprises approximately 17% $^4G_{7/2}$ and 17% $^2K_{15/2}$). The *SLJ* labels are, however, the same as for Er^{3+} in $Cs_3Lu_2Br_9$.[27] The electronic ground state of Er^{3+} in the elpasolite lattice is $^4I_{15/2}$ $a\Gamma_8$ (the subscript u is omitted throughout). In Fig. 1, we have inserted circles to denote the luminescent states of $ErCl_6^{3-}$ to show that the emission spectra of Er^{3+} in elpasolite lattices are rich and well resolved.

A. Absorption spectra

In order to confirm the energy-level assignments from luminescence, we have made a preliminary examination of the ultraviolet absorption spectrum of $Cs_2NaErCl_6$. Transitions to pure electronic excited crystal field states Γ_i ($\Gamma_8 \rightarrow \Gamma_i$, where $i=6-8$) are all potentially allowed by the magnetic dipole mechanism, and appear as zero-phonon lines in the absorption spectra. The vibronic sideband of each transition is identified from the characteristic vibrational energies in Table I, with confirmation from the appearance of vibrational hot bands at elevated temperatures. Furthermore, hot electronic transitions, involving the first excited states at 25 and/or 57 cm^{-1}, are also prominent in many cases above 10 K.

Selected absorption spectra are shown in Fig. 2, with the terminal states being identified for prominent bands. The derived energy levels are listed in Table II. When all of the crystal field levels of a given multiplet term can be identified, then the relative ordering of the symmetry representations follows the calculation. In some cases the spectra consist of many overlapping bands, the features are very weak, or emission bands are superimposed upon the background. Un-

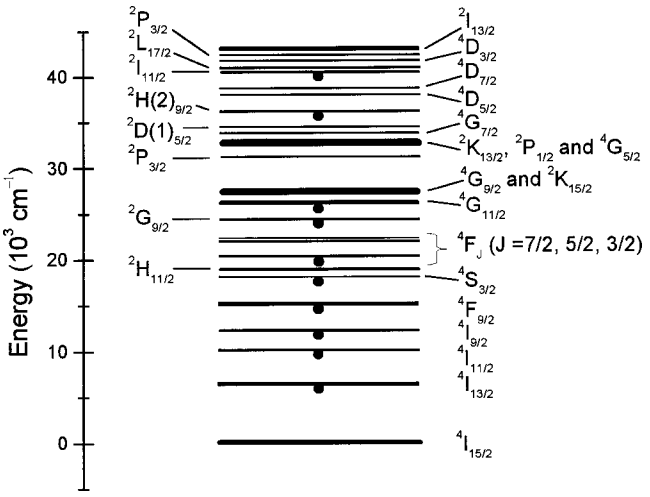

FIG. 1. Energy levels of Er^{3+} in $Cs_2NaErCl_6$ below 44 000 cm^{-1}. Luminescent levels are indicated. Under the conditions of our experiments, no luminescence has been observed from $^2P_{3/2}$ at 31 367 cm^{-1}, but would be expected if this level is suitably populated.

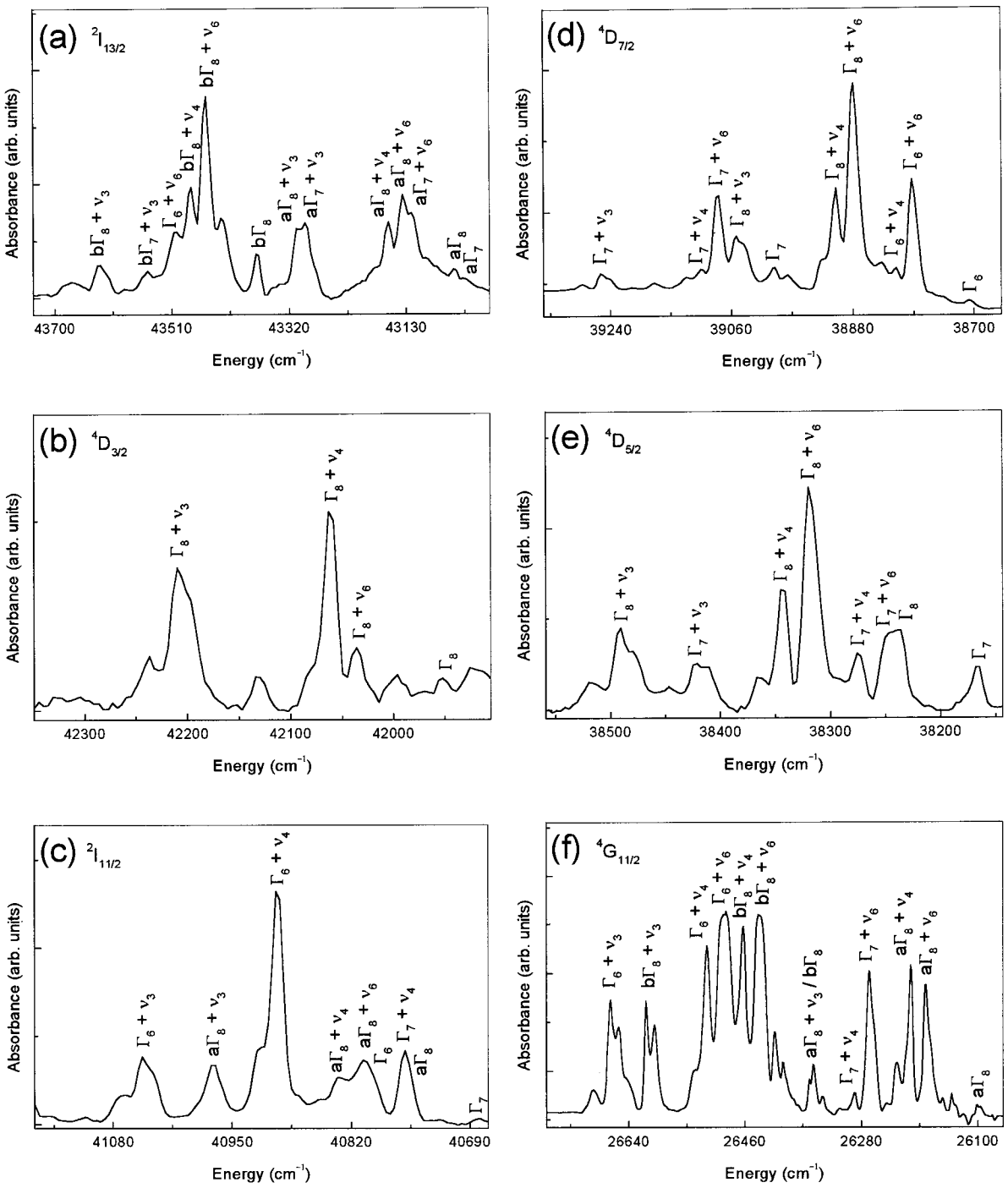

FIG. 2. Selected 10-K absorption spectra of $Cs_2NaErCl_6$. All transitions originate from $^4I_{15/2}\, a\Gamma_8$, and the terminal multiplet states, and crystal field (vibronic) levels are as indicated.

ambiguous assignments are then not always possible, and the tentative locations of energy levels are given in parentheses in Table II.

Altogether, 58 crystal field energy levels have been firmly assigned, with a further 18 tentative levels. The previous assignments[23] given for 41 levels below 27 400 cm^{-1} are essentially confirmed, although minor recalibrations have been made for seven of these highest-energy levels. The most recent energy-level data set[14] of 40 levels for Er^{3+} in $Cs_2NaErCl_6$ was reportedly based upon earlier studies,[18,28] although 24 (27) of the levels are identical with those of Ref. 23 (Ref. 29). In the latter study,[14] only two levels were reported above 27 000 cm^{-1}. One of these, $^2H(2)_{9/2}\, a\Gamma_8$, has since been reassigned from emission spectra,[2] approximately 100-cm^{-1} higher in energy.

B. Luminescence spectra

Under 273.9-nm (36 499-cm^{-1}) excitation of $Cs_2NaErCl_6$, emission is observed from the $^2H(2)_{9/2}$ and

TABLE II. Experimental and calculated energy levels for Er^{3+} in $Cs_2NaErCl_6$.[a]

$^{2S+1}L_J$	Irreducible representation[b]	Experiment[c]	Calculation $E1$	Δ	Calculation $E2$	Δ
$^4I_{15/2}$	$a\Gamma_8$	0	−18	18	−20	20
	Γ_7	25	17	8	13	12
	$b\Gamma_8$	57	44	13	41	16
	Γ_6	259	258	1	254	5
	$c\Gamma_8$	287	286	1	283	4
$^4I_{13/2}$	Γ_6	6 492	6 494	−2	6 495	−3
	$a\Gamma_8$	6 517	6 522	−5	6 523	−6
	$a\Gamma_7$	6 532	6 539	−7	6 539	−7
	$b\Gamma_8$	6 682	6 698	−16	6 697	−15
	$b\Gamma_7$	6 686	6 703	−17	6 702	−16
$^4I_{11/2}$	Γ_6	10 166	10 152	14	10 167	−1
	$a\Gamma_8$	10 174	10 164	10	10 175	−1
	Γ_7	10 238	10 250	−12	10 240	−2
	$b\Gamma_8$	10 238	10 253	−15	10 243	−5
$^4I_{9/2}$	$a\Gamma_8$	12 357	12 315	42	12 331	26
	Γ_6	12 422	12 438	−16	12 421	1
	$b\Gamma_8$	12 502	12 492	10	12 486	16
$^4F_{9/2}$	$a\Gamma_8$	15 152	15 165	−13	15 168	−16
	$b\Gamma_8$	15 246	15 267	−21	15 268	−22
	Γ_6	15 337	15 344	−7	15 344	−7
$^4S_{3/2}$	Γ_8	18 265	18 273	−8	18 274	−9
$^2H(2)_{11/2}$	$a\Gamma_8$	19 010	19 049	−39	19 012	−2
	Γ_7	19 048	19 071	−23	19 049	−1
	$b\Gamma_8$	19 137	19 129	8	19 158	−21
	Γ_6	19 174	19 156	18	19 198	−24
$^4F_{7/2}$	Γ_6	20 374	20 381	−7	20 382	−8
	Γ_8	20 446	20 444	2	20 445	1
	Γ_7	20 467	20 452	15	20 452	15
$^4F_{5/2}$	Γ_8	22 056	22 072	−16	22 072	−16
	Γ_7	22 135	22 132	3	22 131	4
$^4F_{3/2}$	Γ_8	22 445	22 440	5	22 440	5
$^2G_{9/2}$ + $^4F_{9/2}$	$a\Gamma_8$	24 425	24 374	51	24 391	34
	Γ_6	24 459	24 495	−36	24 482	−23
	$b\Gamma_8$	24 519	24 522	−3	24 518	1
$^4G_{11/2}$	$a\Gamma_8$	26 098	26 115	−17	26 093	5
	Γ_7	26 183	26 195	−12	26 183	0
	$b\Gamma_8$	26 354	26 321	33	26 342	12
	Γ_6	26 408	26 373	33	26 399	9
$^4G_{9/2}$	Γ_6	(27 179)	27 185		27 172	
	$a\Gamma_8$	27 220	27 218	2	27 216	4
	$b\Gamma_8$	27 259	27 258	1	27 262	−3
$^2K_{15/2}$	$a\Gamma_8$	27 365	27 383	−18	27 381	−16
	$b\Gamma_8$	27 459	27 477	−18	27 476	−17
	Γ_7	27 504	27 546	−42	27 545	−41
	$c\Gamma_8$	(27 704)	27 742		27 734	
	Γ_6	27 775	27 750	25	27 749	26
$^4G_{7/2}$	Γ_7	(27 966)	27 796		27 775	
$^2K_{15/2}$	Γ_8	(27 981)	27 921		27 910	
	Γ_6	(28 044)	27 957		27 948	
$^2P_{3/2}$	Γ_8	31 367	31 357	10	31 357	10
$^2K_{13/2}$	Γ_6	32 613	32 595	18	32 597	16
	Γ_8	32 676	32 644	32	32 645	31

TABLE II. (Continued)

$^{2S+1}L_J$	Irreducible representation[b]	Experiment[c]	Calculation $E1$	Δ	Calculation $E2$	Δ
	Γ_7	(32 761)	32 702		32 704	
$^2P_{1/2}$	Γ_6		32 889		32 888	
$^4G_{5/2}$	Γ_8		32 911		32 912	
$^2K_{13/2}$	Γ_7		32 936		32 937	
	Γ_8		33 028		33 027	
$^4G_{5/2}$	Γ_7	(33 102)	33 213		33 213	
$^4G_{7/2}$	Γ_6	(33 750)	33 737		33 744	
	Γ_8		33 810		33 816	
	Γ_7	(33 832)	33 936		33 940	
$^2D(1)_{5/2}$	Γ_7	(34 552)	34 552		34 552	
	Γ_8	34 635	34 632	2	34 631	4
$^2H_{9/2}$	$a\Gamma_8$	36 224	36 241	−17	36 239	−15
	Γ_6	36 309	36 318	−9	36 300	9
	$b\Gamma_8$	(36 412)	36 357		36 395	
$^4D_{5/2}$	Γ_7	38 164	38 164	0	38 165	−1
	Γ_8	38 234	38 251	−17	38 252	−18
$^4D_{7/2}$	Γ_6	38 705	38 743	−38	38 741	−36
	Γ_8	38 790	38 807	−17	38 804	−14
	Γ_7	38 993	38 945	48	38 942	51
$^2I_{11/2}$	Γ_7	40 668	40 654	14	40 650	18
	$a\Gamma_8$	(40 750)	40 696		40 693	
	Γ_6	(40 815)	40 735		40 734	
	$b\Gamma_8$	(40 914)	40 746		40 745	
$^2L_{17/2}$	Γ_7	(41 187)	41 205		41 205	
	$a\Gamma_8$		41 219		41 219	
	$a\Gamma_6$	41 270	41 252		41 252	
	$b\Gamma_8$		41 307		41 307	
	$c\Gamma_8$		41 323		41 323	
	$b\Gamma_6$	(41 417)	41 331		41 330	
$^4D_{3/2}$	Γ_8	41 965	41 946	19	41 949	16
$^2P_{3/2}$	Γ_8	(42 518)	42 510		42 510	
$^2I_{13/2}$	$a\Gamma_7$	(42 693)	43 027		43 030	
	$a\Gamma_8$	(43 048)	43 045		43 049	
	$b\Gamma_7$		43 314		43 317	
	$b\Gamma_8$	(43 362)	43 334		43 336	
	Γ_6	43 388	43 391	−3	43 392	−4

[a]Calculation $E1$ is performed with normal tables of U^k; calculation $E2$ with $\langle ^2H(2)\|U^4\|^2H(2)\rangle = 0.85$ instead of 0.495 (i.e., multiplied by a factor of 1.717).

[b]Irreducible representation in O_h molecular point-group symmetry.

[c]Experimental energy.

several lower multiplet terms.[2] Other impurity species, besides $ErCl_6^{3-}$, are excited under 217.8-nm (45 899-cm^{-1}), 240-nm (41 741-cm^{-1}), and 266-nm (36 583-cm^{-1}) excitation. We therefore focus our results upon the 199.8 (50 034-cm^{-1}) excited spectrum of $Cs_2NaErCl_6$, in which luminescence is observed from $^2I_{11/2}$ and lower levels. The 192.2-nm (52 012-cm^{-1}) and 199.8-nm excited spectra of Cs_2NaYCl_6:Er are similar to each other, and are described, where relevant, for comparison with the spectra of $Cs_2NaErCl_6$.

C. Luminescence from $^2I_{11/2}$

The highest-energy transition of $Cs_2NaErCl_6$ observed under 199.8-nm excitation is a group of bands between 40 668 and 40 095 cm^{-1}. The span of 573 cm^{-1} is associated with a phonon energy of 286 cm^{-1} plus an electronic energy of 287 cm^{-1}, corresponding to the highest-energy (longitudinal-optic) component of the ν_3 vibration, and the highest-energy crystal field level $c\Gamma_8$ of the electronic ground state. From this, and lower transitions, the $^2I_{11/2}$ Γ_7 state is assigned at $40\,668 \pm 12$ cm^{-1}. The gap to the next-

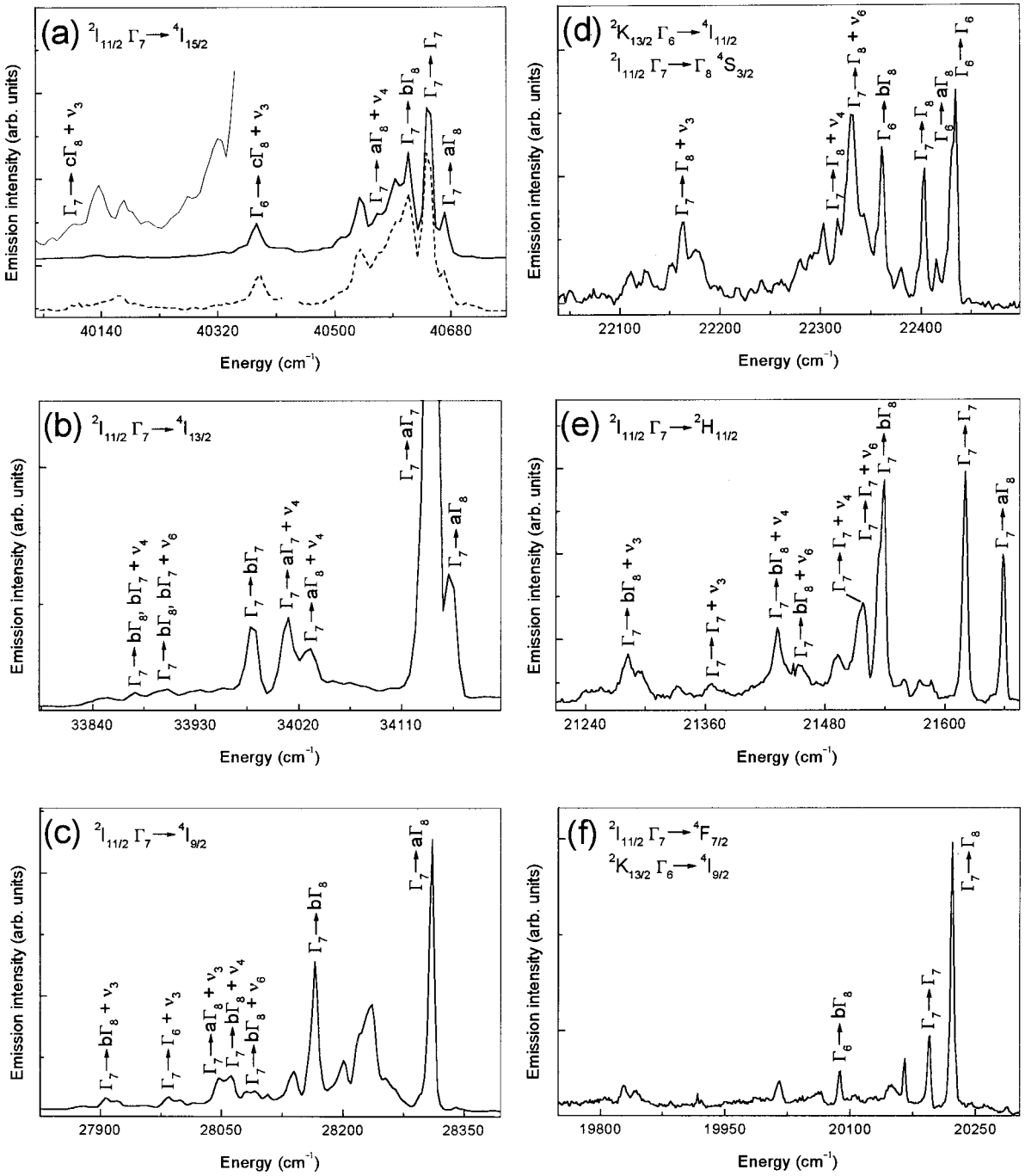

FIG. 3. Emission transitions of $^2I_{11/2}\ \Gamma_7$ in the 199.8-nm excited emission spectra of $Cs_2NaErCl_6$ (solid lines) and 192.2-nm excited spectra of Cs_2NaYCl_6:Er (dotted line) at 10 K.

lowest level $^4D_{7/2}\ \Gamma_7$ is 1675 cm^{-1}, i.e., spanned by six phonons, so that radiative processes are expected to dominate over nonradiative ones.[30] The strongest bands in this $^2I_{11/2}\ \Gamma_7 \rightarrow {}^4I_{15/2}$ transition, Fig. 3(a), are magnetic dipole allowed zero-phonon lines, and the absence of the $\Gamma_7 \rightarrow \Gamma_6$ zero-phonon line is as expected from the O_h site selection rules. The next-lowest group of bands in the 199.8-nm excited spectrum corresponds to the $^2H(2)_{9/2}\ a\Gamma_8 \rightarrow {}^4I_{15/2}$ transition, which has been described elsewhere.[2] Figure 3(b) shows the next transition from $^2I_{11/2}$, between 34 162 and 33 860 cm^{-1}, terminating upon $^4I_{13/2}$ levels. Again, most of the intensity arises from magnetic dipole allowed transitions, with $^2I_{11/2}\ \Gamma_7 \rightarrow a\Gamma_7\ {}^4I_{13/2}$ particularly intense. The transition $^2I_{11/2}\ \Gamma_7 \rightarrow {}^4I_{9/2}$ is shown in Fig. 3(c). The magnetic dipole allowed zero-phonon lines $\Gamma_7 \rightarrow a\Gamma_8$, $b\Gamma_8$ are prominent, with $\Gamma_7 \rightarrow \Gamma_6$ missing. The location of the latter is readily identified from its associated vibronic structure. The weak transition $^2I_{11/2}\ \Gamma_7 \rightarrow {}^4F_{9/2}$ is observed to low energy of the intense $^4G_{11/2}\ a\Gamma_8 \rightarrow {}^4I_{15/2}$ transition. Again, the zero-phonon lines $\Gamma_7 \rightarrow a\Gamma_8$, $b\Gamma_8$ are prominent, with $\Gamma_7 \rightarrow \Gamma_6$ missing, but identified from vibronic structure. The $^2I_{11/2}\ \Gamma_7 \rightarrow {}^4S_{3/2}$ transition is identified from the associated ν_3, ν_4, and ν_6

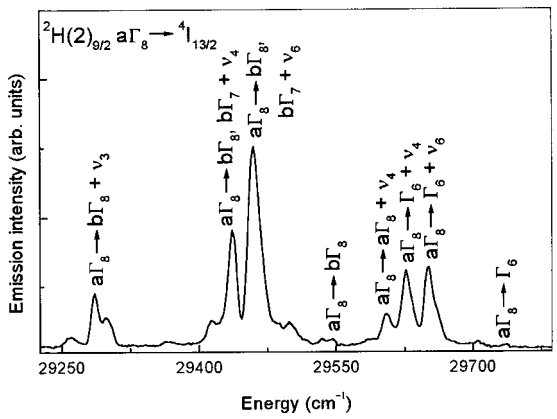

FIG. 4. Up-converted $^2H(2)_{9/2} \rightarrow {}^4I_{13/2}$ emission spectrum of $Cs_2NaErCl_6$ under 488-nm pulsed laser excitation at 10 K.

vibronic origins, but overlaps with bands in the $^2K_{13/2}\ \Gamma_6 \rightarrow {}^4I_{11/2}$ transition, Fig. 3(d). The three magnetic dipole allowed zero-phonon lines of the $^2I_{11/2}\ \Gamma_7 \rightarrow {}^2H_{11/2}$ transition are clearly identified [Fig. 3(e)]. The $^2I_{11/2}\ \Gamma_7 \rightarrow {}^4F_{7/2}$ transition is coincident with $^2K_{13/2}\ \Gamma_6 \rightarrow {}^4I_{9/2}$ and the bands are distinguished in the spectrum of $Cs_2NaErCl_6$, Fig. 3(f). Only the two prominent magnetic dipole transitions $^2I_{11/2}\ \Gamma_7 \rightarrow \Gamma_8$, $\Gamma_7\ {}^4F_{7/2}$ are evident in the spectrum of Cs_2NaYCl_6:Er. The transition $^4F_{7/2}\ \Gamma_6 \rightarrow {}^4I_{15/2}$ is also expected in this region but is too weak to be observed. Two sharp weak bands (not shown in the figure) are observed at 18 622 and 18 541 cm^{-1}, which correspond to the zero-phonon lines of the $^2I_{11/2}\ \Gamma_7 \rightarrow \Gamma_8$, $\Gamma_7\ {}^4F_{5/2}$ transition. The transition terminating upon $^4F_{3/2}\ \Gamma_8$ is masked by the intense $^4S_{3/2}\ \Gamma_8 \rightarrow {}^4I_{15/2}$ transition. The zero-phonon lines of the $^2I_{11/2}\ \Gamma_7 \rightarrow {}^2G_{9/2}$ transitions are clearly observed, with the strongest feature, at 16 254 cm^{-1}, corresponding to $\Gamma_7 \rightarrow a\Gamma_8\ {}^2G_{9/2}$. The transition from $^2I_{11/2}\ \Gamma_7$ to $^4G_{11/2}$ is weak, but with $\Gamma_7 \rightarrow \Gamma_7$ prominent at 14 497 cm^{-1}. Several other transitions overlap in this spectral region.

D. Luminescence from $^2H(2)_{9/2}$

The luminescence from this term to lower ones is intense under 273.9-nm excitation of $Cs_2NaErCl_6$, and has previously been described.[2] The gap from $^2H(2)_{9/2}$ to the next-lowest level is spanned by six phonons. Hasan *et al.*[14] have reported the two-photon excited emission from $^2H(2)_{9/2}$, using a pulsed laser at 18 270 cm^{-1}, with energy width approximately 0.1 cm^{-1}. From absorption and emission spectra, we assign $^2H(2)_{9/2}\ a\Gamma_8$ at $36\,224 \pm 12\ cm^{-1}$. Our energy-level results (Table II) show that there is no electronic level at $2 \times 18\,270 = 36\,540\ cm^{-1}$, but the population of a gerade vibronic state is feasible. We succeeded in obtaining up-conversion to $^2H(2)_{9/2}$ using pulsed laser excitation of approximately 19 130 cm^{-1}, or several different (higher) energies. Figure 4 shows the 488-nm excited spectrum, corresponding to $^2H(2)_{9/2} \rightarrow {}^4I_{13/2}$. In this case, the up-conversion mechanism either corresponds to excited-state absorption or to an energy-transfer process, both involving $^4S_{3/2}$.

E. Luminescence from $^2K_{13/2}$

The $^2K_{13/2}\ \Gamma_6$ level has been identified from the absorption spectrum at 32 613 cm^{-1}, with an energy gap of 1246 cm^{-1} (i.e., five phonons) to the next-lowest level $^2P_{3/2}$. The transition to the electronic ground state from $^2K_{13/2}$ is observed in the 199.8-nm excited spectrum of $Cs_2NaErCl_6$, but not in the 273.9-, 266-, 239.5-, or 217.8-nm excited spectra, nor in the 192.2- and 199.8-nm excited spectra of Cs_2NaYCl_6:Er. In the 199.8-nm excited emission spectrum of $Cs_2NaErCl_6$, two medium intensity, sharp bands at 32 605 and 32 549 cm^{-1} are assigned to the transitions to the $a\Gamma_8$ and $b\Gamma_8\ {}^4I_{15/2}$ terminal levels, with that for the Γ_7 level being absent, as expected for an octahedral Er^{3+} site. The remaining structure of this transition is much weaker, except for $\Gamma_6 \rightarrow \Gamma_7 + \nu_4$, ν_3. The next transition from $^2K_{13/2}\ \Gamma_6$ is expected at approximately 6500 cm^{-1} to lower energy, i.e., below 26 000 cm^{-1}. This region is complex due to several overlapping transitions. Figure 5(a) shows the 199.8-nm excited spectrum of $Cs_2NaErCl_6$, with the zero-phonon lines of transitions to the $a\Gamma_8$ and $b\Gamma_8\ {}^4I_{13/2}$ levels, and other vibronic transitions terminating on $^4I_{13/2}$ marked. The remaining bands correspond to the $^4G_{11/2}\ a\Gamma_8 \rightarrow {}^4I_{15/2}$ transition and are assigned in Figs. 5(b) and 5(d). Figure 5(c) shows the same spectral region under 273.9-nm excitation, which populates $^2H(2)_{9/2}$, but not $^2K_{13/2}$, so that most of the bands are associated with $^2H(2)_{9/2}\ a\Gamma_8 \rightarrow {}^4I_{11/2}$, as indicated, but the remaining (unmarked) features correspond to the $^4G_{11/2}\ a\Gamma_8 \rightarrow {}^4I_{15/2}$ transition.

The transition from $^2K_{13/2}$ to $^4I_{11/2}$ is shown in Fig. 3(d), with the zero-phonon lines $\Gamma_6 \rightarrow \Gamma_6$, $a\Gamma_8$, $b\Gamma_8$ clearly identified. The transition to $^4I_{9/2}$ is overlapped by $^2I_{11/2}\ \Gamma_7 \rightarrow {}^4F_{7/2}$, Fig. 3(f), but the $\Gamma_6 \rightarrow b\Gamma_8$ zero-phonon line and vibronic structure are clearly resolved. The $^2K_{13/2} \rightarrow {}^4F_{9/2}$ transition is largely masked by $^4S_{3/2} \rightarrow {}^4I_{15/2}$, and $^2K_{13/2} \rightarrow {}^4S_{3/2}$ by $^2G_{9/2}\ a\Gamma_8 \rightarrow {}^4I_{11/2}$.

F. Luminescence from $^2P_{3/2}$

The $^2P_{3/2}\ \Gamma_8$ level has been identified from the absorption spectrum at 31 367 cm^{-1}, with an energy gap $>3000\ cm^{-1}$ above $^2K_{15/2}$ (Table II). The transitions from this level are not conclusively observed under the conditions of our experiments. It is noted that the cross relaxation $^2P_{3/2}\ \Gamma_8 + {}^4I_{15/2}\ a\Gamma_8 \rightarrow {}^2H(2)_{11/2}\ a\Gamma_8 + {}^4I_{9/2}\ a\Gamma_8$ is resonant within the error of our measurements. Under 273.8-nm excitation, although intense emission is observed from $^2H(2)_{9/2}\ \Gamma_8$, none is evident from $^2P_{3/2}\ \Gamma_8$. This is because there is a level bypassing process, in the nonradiative population pathway of the latter from the former, involving the cross relaxation of the next (luminescent) level above $^2P_{3/2}\ \Gamma_8$ (i.e., $^2K_{13/2} \rightarrow {}^4G_{11/2}$). This could also contribute to the observation of emission *only* from $^4G_{11/2}$ and lower levels in this case.

G. Luminescence from $^4G_{11/2}$ and $^2G_{9/2}$

The $^4G_{11/2}\ a\Gamma_8 \rightarrow {}^4I_{15/2}$ transition [Figs. 5(b) and 5(d)] is mainly vibronic in character. All of the zero-phonon lines in the transition to $^4I_{13/2}$ are clearly observed, between 19 606

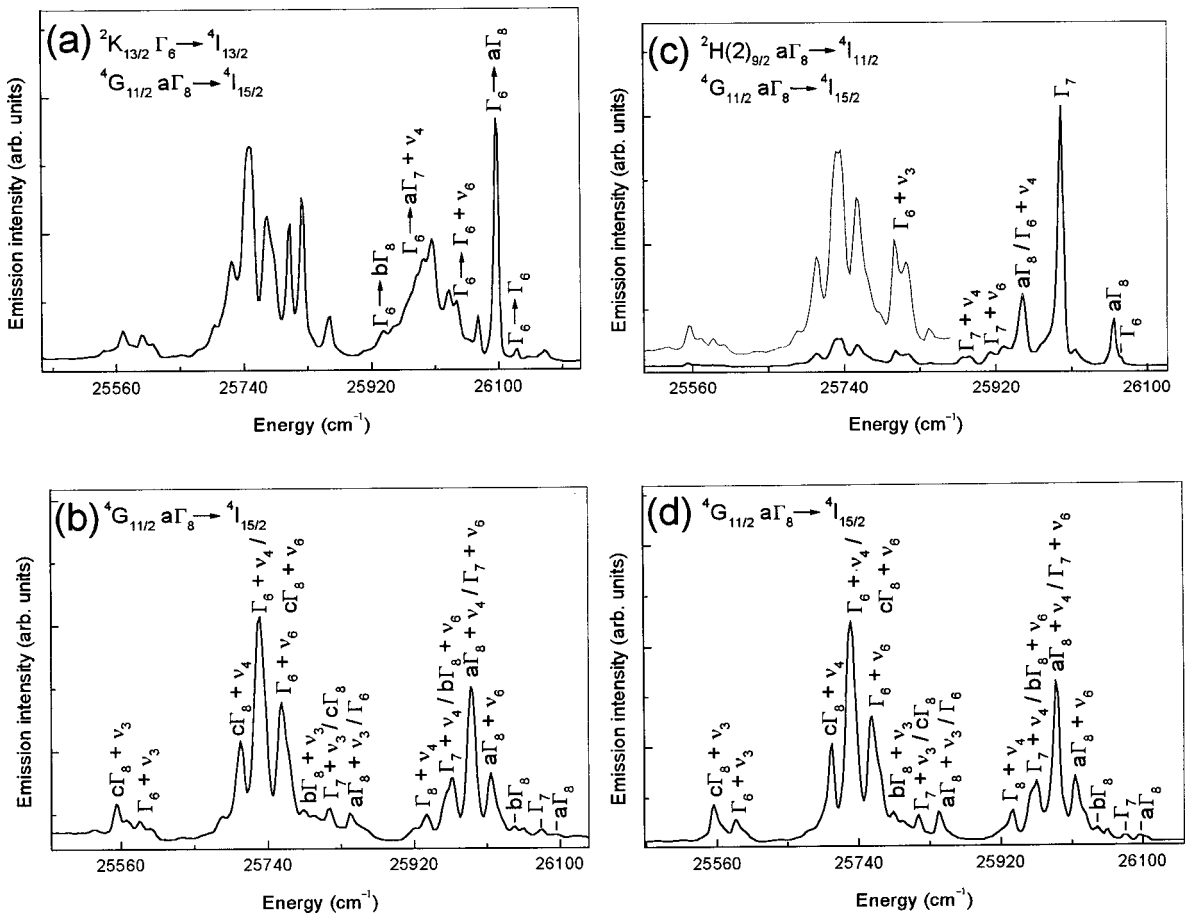

FIG. 5. Emission spectra of $ErCl_6^{3-}$ at 10 K in the region between 26 200 and 25 500 cm^{-1} using different excitation lines: (a) 199.8-, (b) 239.5, and (c) 273.9-nm excited spectra of $Cs_2NaErCl_6$; (d) 199.8-nm excited spectrum of Cs_2NaYCl_6Er.

and 19 416 cm^{-1}, with $a\Gamma_8 \rightarrow a\Gamma_7$ most prominent. Most of the vibronic structure in this transition is totally absorbed by the $^4I_{15/2} \rightarrow {}^2H_{11/2}$ transition.

The $^2G_{9/2}\ a\Gamma_8 \rightarrow {}^4I_{15/2}$ transition is unusual because strong, sharp bands due to exciton traps are observed at 10 K, at different energies under different excitation conditions. These bands are absent in the 488-nm excited up-conversion emission of $Cs_2NaErCl_6$, and from the 199.8-nm excited emission spectrum of Cs_2NaYCl_6:Er. Bands due to trap emission are also clearly identified in the $^2G_{9/2}\ a\Gamma_8 \rightarrow {}^4I_{11/2}$ spectrum, between 14 264 and 14 215 cm^{-1}. Campbell *et al.*[13] have observed additional peaks in the $^2G_{9/2}\ a\Gamma_8 \rightarrow {}^4I_{15/2}$ spectrum of Cs_2NaYCl_6:Er under excitation at 651 nm at 1.2 K, but not at 4.2 K, or under 364-nm excitation at 1.2 K. The defect sites have been associated with the presence of oxychloride ions in the deliquescent crystals.[13] It was concluded in Ref. 13 that the migration of energy throughout the lattice, and trapping at defect sites, occur only in the lower-energy states ($^4S_{3/2}$, $^4F_{9/2}$, $^4I_{9/2}$). Our results show that this is clearly not the case, since trap bands are also observed under ultraviolet excitation. We note that the nature of the defect sites could also include Er^{3+} ions adjacent to other lanthanide ion chromophores which efficiently absorb the laser excitation energy (including $f \rightarrow d$ excitations), and subsequently transfer energy to the Er^{3+} trap site. Since the symmetry of the acceptor Er^{3+} site point group is lowered from octahedral symmetry to a noncentrosymmetric site point group, the Er^{3+} trap site emission acquires electric dipole character in the pure electronic transitions.

IV. CRYSTAL FIELD ANALYSIS

A. Analysis of new data set

As noted previously, the most recent energy-level parametrization[14] (using 23 atomic and crystal field parameters) of Er^{3+} in $Cs_2NaErCl_6$ utilized 40 crystal field levels, but with only two of these above 27 000 cm^{-1}. The initial assignments for the 58 experimental energy levels, spanning up to 43 000 cm^{-1}, determined in the present study were made by reference to the previous energy-level parametrization in Ref. 23. Then, a new refinement of parameters was made in order to improve both the fitting of securely assigned levels, and also the understanding of a further 20 ''uncertain'' energy-level assignments. Following these revised energy-level calculations, six of these uncertain levels were deleted, six reassigned to other irreducible representations, and eight remained unchanged. However, a further three new levels were then assigned as ''uncertain,'' making a total of 18 at present. The energy-level symmetry representation assignments for the original 58 levels remained unchanged throughout, and these were the only levels fitted in the new calculations now described.

TABLE III. Empirical Hamiltonian parameters of Er^{3+} in $Cs_2NaErCl_6$. Calculation $E1$: normal fit with 58 levels. Values of the mean deviation are for the global fit (a), the fit on quartets (b), and that on doublets (c), respectively. m: multiplying factor of $\langle {}^2H(2)\|U^4\|{}^2H(2)\rangle$. Calculation $E2$: fit utilizing $m=1.717$, that is, $\langle {}^2H(2)\|U^4\|{}^2H(2)\rangle = 0.85$ instead of 0.495. Parameters in square brackets were varied by steps and then held constant during the refinement of the other parameters.

Parameter	Calculated $E2$	Calculated $E1$	Reference 23
F^2	96 715 (66)	96 717 (80)	97 273
F^4	67 400 (111)	67 374 (134)	69 131
F^6	47 553 (100)	47 541 (122)	48 340
α	17.6 (0.4)	17.6 (0.5)	[15.90]
β	−661 (17)	−655 (21)	[−623]
γ	[2500]	[2500]	[2017]
T^2	[120]	[120]	[300]
T^3	48 (8)	50 (10)	[48]
T^4	58 (9)	56 (10)	[18]
T^6	−292 (28)	−286 (34)	[−342]
T^7	201 (28)	191 (34)	[214]
T^8	[176]	[176]	[449]
M^0	4.0 (0.2)	4.1 (0.3)	[4.5]
P^2	[510]	[510]	[667]
ζ	2363 (2)	2363 (3)	2362
B_0^4	1543 (48)	1555 (60)	1492
B_0^6	158 (17)	154 (21)	163
m	1.717	1	
N	58 (a) 39 (b) 19 (c)	58 (a) 39 (b) 19 (c)	41
σ	20.4 18.0 24.6	16.8 15.0 19.9	18.4

The measured energy levels were fitted to the standard model Hamiltonian[31–34] involving a total of 18 parameters. These comprise 16 free ion parameters, out of which 15 control the interaction between term multiplets: the Slater parameters F^k $(k=0, 2, 4, 6)$; the configuration-interaction parameters α, β, and γ; the three-body parameters T^i $(i=2, 3, 4, 6, 7, 8)$; and the parameters of magnetic interactions M^k $[k=0(2, 4); M^2=0.56M^0;\ M^4=0.38M^2]$ and P^k $[k=2(4, 6); P^4=0.75P^2; P^6=0.5P^2]$. The remaining free ion parameter is the spin-orbit coupling constant ζ, which controls the interaction between SLJ levels. Two more parameters are required to account for the crystal field interaction in octahedral symmetry: B_0^4 and B_0^6. The Wybourne spherical tensorial notation is adopted herein, and in the cubic environment, $B_4^4 = \pm B_0^4(5/14)^{1/2}$ and $B_4^6 = \mp B_0^6(7/2)^{1/2}$.

The $4f^{11}$ configuration comprises 17 terms: ^4S, ^4D, ^4F, ^4G, ^4I, ^2P, ^2D (1, 2), $^2F(1,2)$, $^2G(1,2)$, $^2H(1,2)$, ^2I, ^2K, and ^2L. The 58 experimentally observed levels belong to the 11 terms ^4I, ^4F, ^4S, $^2H(2)$, ^4G, ^2K, ^2P, $^2D(1)$, ^4D, ^2I, and ^2L. The six remaining terms $^2H(1)$, $^2D(2)$, $^2F(1,2)$, and $^2G(1,2)$ lie above 43 000 cm^{-1}. It is therefore impossible to fit the whole group of 15 free ion parameters acting between terms, even if small amounts of the hitherto unobserved higher levels are mixed with the lower ones. Actually, fits operated by varying all the parameters were not very efficient. Parameter γ, for instance, was strongly correlated with other parameters, as shown by its very large standard deviation. The optimum value for γ was determined by ascribing to it a set of fixed values and by performing, each time, the fit of the other variable parameters. T^2, T^8, and P^2 were also fixed in the final steps of the refinement. The 14 variable parameters were F^k $(k=0, 2, 4, 6)$, α, β, T^i $(i=3, 4, 6, 7)$, M^k $(k=0)$, ζ, B_0^4, and B_0^6. The experimental and calculated energy levels are listed in Table II, with the parameters and mean deviations in Table III (in column $E1$). For comparison, Table III also includes the parameters obtained in a previous fit[23] on 41 experimental levels, ranging up to 27 374 cm^{-1}. The mean deviation for 58 levels obtained in the present work amounts to 20.4 cm^{-1}, compared with 18.4 cm^{-1} in the earlier work.[23] However if the parameters from Ref. 23 are applied to the present, entire set of experimental data, the mean deviation then soars up to 40 cm^{-1}. In particular, the calculated energy of the highest $^4D_{7/2}$ level is 137-cm^{-1} lower than its experimental value, 38 993 cm^{-1}. The differences between the crystal field parameter values of column $E1$ and Ref. 23 cannot account for this difference, since they only produce a 0.2-cm^{-1} change of the mean deviations. The large difference between the two fits is essentially due to the parameters for the free ion interaction. The higher levels could not be fitted with the previous[23] γ value. Optimum results were obtained with $\gamma = 2500$ cm^{-1}, compared with 2017 cm^{-1} in the earlier work.[23]

Separate fits were made to the quartet levels, and to the doublet levels, by varying the fourth and sixth degree crystal field parameters alone. The mean deviation for the 39 quartet states was equal to 18.0 cm^{-1} and that for the 19 doublet states was 24.6 cm^{-1}. The fourth degree crystal field parameter turned out to be 1.07 times greater for the quartets than

for the doublets. However, it is mentioned that the standard deviations of these parameters are large.

Considering only the securely assigned levels, then the most poorly fitted levels are from the terms $^4I_{9/2}$, $^2H(2)_{11/2}$, $^4F_{9/2}$, $^4G_{11/2}$, and $^4D_{7/2}$ (with mean deviations of 28.2, 25.9, 36.1, 26.2, and 32.9 cm^{-1}, respectively). A bad adjustment of the baricenters accounts for part of these large deviations (despite the large number of free ion parameters). Regarding the ''uncertain'' levels, the present calculations give more credence to the proposed assignments for $^2I_{13/2}$ [refer to Fig. 2(a) and Table II].

It is well established that the $^2H(2)$ multiplet of the $4f^3$ and $4f^{11}$ configurations belongs to a set of ''abnormal'' terms existing among the series of rare-earth ions, for which the crystal field levels can seldom be satisfactorily fitted by the standard procedure. This fact is particularly conspicuous for Nd^{3+}.[35] It is attenuated for Er^{3+}, since a part of the discrepancy is absorbed by other multiplets such as $^4I_{9/2}$, $^4F_{9/2}$, and $^4G_{11/2}$, which are strongly coupled to $^2H(2)_{9/2,11/2}$ by the very large spin-orbit coupling interaction, but the trend is the same. For instance, the calculated splitting of the $^2H(2)_{11/2}$ levels in Er^{3+} compounds is always smaller than experimental splitting. It has been shown[35,36] for the case of Nd^{3+} that this discrepancy is connected with the strength of the fourth-order crystal field, and that it can be fairly well corrected by an empirical modification of the $\langle ^2H(2)\|U^4\|^2H(2)\rangle$ reduced matrix element. A crystal field analysis for a series of ten Nd^{3+} systems showed that the best multiplying factor for the correction was close to 0.25.[36] In other words, $\langle ^2H(2)\|U^4\|^2H(2)\rangle$ is replaced by $(1-0.75)\times\langle ^2H(2)\|U^4\|^2H(2)\rangle$. It turned out a little later after the development of the correlation crystal field[37] (CCF) that this correction had approximately the same effect as the $g^4_{10,A}$ operator of the CCF. If the perturbing term is due to two-electron effects, then it does not change sign in the second half of the rare-earth series while the reduced matrix element $\langle ^2H(2)\|U^4\|^2H(2)\rangle$ does, and the resulting term should be $(-1-0.75)\times\langle ^2H(2)\|U^4\|^2H(2)\rangle$. In other words the reduced matrix element of the Nielson and Koster tables[37] is multiplied by 1.75 (while it is multiplied by 0.25 for Nd^{3+}). A mean multiplying factor equal to 1.6 was applied in the parametric simulation of energy levels of Er^{3+} in Er_2O_2S, LaF_3, $LiYF_4$, and Y_2O_3,[38] with an improvement of the mean deviation ranging from 9% to 30%. The empirical correction is easy to apply since it suffices to replace the value of $\langle ^2H(2)\|U^4\|^2H(2)\rangle = 0.495\,023\,4$ in Nielson and Koster's tables[39] by 0.123 755 9 for Nd^{3+} and 0.866 291 0 for Er^{3+}. The correction is efficient for $^2H(2)_{11/2}$ and $^2H(2)_{9/2}$ and for those levels which are coupled to them by spin-orbit interaction, such as $^4I_{9/2}$, $^4F_{9/2}$, and $^4G_{11/2}$. The same process has been utilized in the present case, and the multiplying factor m of $\langle ^2H(2)\|U^4\|^2H(2)\rangle$ was considered as an additional parameter. As for the parameter *m*, several values were tested, while the other parameters were refined. The value leading to the lowest mean deviation was finally retained. Actually, the final value of m (1.717, hence $\langle ^2H(2)\|U^4\|^2H(2)\rangle = 0.85$) is very close to the one deduced above by reference to Nd^{3+}. Then, in the final fit, the global mean deviation of experimental/calculated energy levels became equal to 16.8 cm^{-1}, with the deviations for quartets and doublets being equal to 15 and 19.9 cm^{-1}, respectively. The final parameter values are listed in Table III, column *E*2, while the calculated energy levels are also included in Table II. The mean deviations for $^4I_{9/2}$, $^2H(2)_{11/2}$, $^4F_{9/2}$, $^4G_{11/2}$, and $^4D_{7/2}$ are then equal to 19.3, 15.6, 23.8, 8.4, and 32.7 cm^{-1}, respectively. It is noteworthy that the calculated $^4D_{7/2}$ splitting is not improved at all since it is not significantly mixed with levels involved by the correction on $\langle ^2H(2)\|U^4\|^2H(2)\rangle$.

B. Comparison with previous energy-level parametrizations of Er^{3+} in crystals

The success of the present energy-level fitting may be judged through the comparison with previous energy-level parametrizations of Er^{3+} systems, by comparing various factors such as the number and extent of the energy levels fitted, the number of parameters utilized, the resulting accuracy, and the validity of the derived parameters. Of course, a prerequisite is the quality of the energy-level data set. In the present study, 58 crystal field levels [total degeneracy (TD) 180] were assigned and fitted, with a further 18 levels (TD 52) being uncertain because of incomplete vibronic fingerprints. We consider that the comparison of data concerning a particular energy level from absorption, emission, and excitation spectra, together with the detailed vibronic fingerprints, have provided a reliable data set. The most extensive, previous assignments of Er^{3+} systems have been made for cases where all crystal field levels entirely comprise Kramers doublets: YAG Er^{3+} (TD 234),[40] and LaF_3 Er^{3+} (TD 254).[41] Some concerns have been raised concerning the correctness of assignments in LaF_3,[42] and also in YAG Er^{3+} all crystal field levels have the same symmetry representation so that transition selection rules do not aid energy-level assignments. With the exception of $Cs_3Lu_2Cl_9$ (Ref. 43) (where 111 levels were assigned from polarized spectra) and the garnet[40] studies, few others have included energy levels higher than 30 000 cm^{-1} in the fitting process, when as mentioned above, the inclusion of predominantly doublet levels would more severely test the quality of the fit. For example, Capobianco *et al.*[44] fitted 59 levels in $YVO_4:Er^{3+}$ at energies $<28\,000$ cm^{-1}; Quagliano *et al.*[45] fitted 67 levels of $CsCdBr_3:Er^{3+}$ with only two of these $>28\,000$ cm^{-1}; Krämer, Güdel, and Schwartz[46] fitted 73 levels of $LaCl_3:Er^{3+}$ with 12 of these $>28\,000$ cm^{-1}. In the case of $Cs_3Lu_2Br_9:Er^{3+}$,[47] although the standard deviation in fitting 87 levels was 19.3 cm^{-1}, a further 13 levels (mainly doublets) not included in the fitting process deviate by an average of 269 cm^{-1} *each* from the calculated energies. In the present study, it is clear that the average error for the 18 uncertain levels (i.e., 21 cm^{-1}) does not differ much from the mean deviation of the fit.

The comparison of the present work with previous studies should also take into account the fact that only two crystal

field parameters have been employed, whereas the number is considerably greater for other systems: nine for YAG and LaF_3, and six for $CsCdBr_3$ and Cs_3LuX_9 (X=Cl,Br). In the other systems mentioned, the values (in cm^{-1}) of the Slater parameters fall in the following ranges: F^2 96 417 (Ref. 46) to 99 394,[40] F^4 67 501 (Ref. 47) to 72 778,[44] and F^6 48 114 (Ref. 46) to 54 010.[41] The present value for F^2 falls within this range, but the magnitudes of F^4 and F^6 are slightly lower (Table III). Our parameter values of α and β are similar to those of other studies, where the ranges (in cm^{-1}) are from 15.95 (Ref. 14) to 18.66,[47] and -509 (Ref. 44) to -727,[47] respectively. More variation is evident, however, for γ, which has sometimes been constrained,[45] since it ranges from 2500 cm^{-1} in the present study to 650 cm^{-1} in Ref. 44. It is clear that the γ parameter is absorbing deficiencies from other parameters in the fit, and can vary wildly if not constrained, just as the values of T^2 (which is quite small in the present calculation) range from 18 (Ref. 47) to 640,[40] in other Er^{3+}-doped systems.

Correlation crystal field (CCF) interactions[14,37,43,45–47] have also been utilized for a phenomenological correction of crystal field effects on abnormal multiplets. The analysis has been restricted to those among the many terms of the CCF Hamiltonian which have large matrix elements within the abnormal states. In Ref. 40, a 2–3-cm^{-1} decrease of the global mean deviation was obtained for crystal field analyses of Er^{3+} doped into garnet systems. This represents a 12%–20% decrease of the overall mean deviation, depending on the investigated garnet. In the present work, utilizing an alternative empirical strategy, the decrease of the global deviation is equal to 18%, which is quite satisfying. The object of employing the CCF interaction[47] has been to correct the ground-state $^4I_{15/2}$ term energies, as well as the anomalous excited $^2H(2)$ multiplet term energies. However it was found that the inclusion of several different CCF parameters actually had little effect upon the fitting of $^4I_{15/2}$ levels.[47]

The crystal field strength is a spherical parameter independent of the crystal symmetry and has known several slightly different formulations.[48–50] The strength parameter[51] S^k is a convenient parameter for comparing the kth-order crystal field interaction of Er^{3+} in various crystalline hosts with very different environments and therefore different reference axes. The comparison (Table IV) is made with respect to uncorrected crystal field parameters, without empirical correction or CCF contributions. We note that the inclusion of this second-order crystal field effect does not, at least in the studies that are quoted here, change significantly the values of the crystal field strength parameters which describe a first-order crystal field effect. For instance, the changes in the magnitude of $k=4$ crystal field strength amount to 1%, 8%, and 0% for garnets[40] $CsCdBr_3$ (Ref. 45) and $Cs_3Lu_2Cl_9$,[43] respectively. For the compounds with Cs^+ cations in Table IV, the $k=4$ and 6 crystal field strengths show an increasing trend from Br to Cl nearest neighbors of Er^{3+}. The expected trend from Cl to F is observed in LaX_3, but a more detailed interpretation of all the trends is outside the scope of the present study. It is noted however, that the crystal field strengths for the dimeric system $Cs_3Lu_2Cl_9$ (where three Cl atoms are shared by two Er^{3+}, each of which are six coordinate) and the system $Cs_2NaErCl_6$ are fairly similar, proving that their environments are not very different either. It is worthwhile considering this point a little further. The vicinity of Er^{3+} in $Cs_2NaErCl_6$ (Ref. 4) and $Cs_3Lu_2Cl_9$ is shown in Figs. 6(a) and 6(b), respectively, where the $Cs_3Lu_2Cl_9$ (Ref. 52) structure has been rotated in order to bring the pseudo-fourth-order axis along the one of the fourfold axes of the $Cs_2NaErCl_6$. The similarity of the Er^{3+} close environments in these two hosts is striking. Starting from the optically active ion in both compounds we find. Six Cl^- neighbors at about 2.5 Å on the apices of an octahedron (a pseudoregular octahedron in the case of $Cs_3Lu_2Cl_9$), and then a Lu^{3+} ion for $Cs_3Lu_2Cl_9$, at about 3.6 Å on the C_3 axis (oblique from upper left to lower right), which constitutes the first important difference. Next come eight and six Cs^+ neighbors for $Cs_2NaErCl_6$ and $Cs_3Lu_2Cl_9$, respectively, at about 4.5 Å. Six out of eight of these Cs^+ ions have a similar arrangement in both structures. The Na^+ ions in $Cs_2NaErCl_6$ are further

TABLE IV. Fourth- and sixth-order crystal field strengths S^k (in cm^{-1}), from various energy level fits for Er^{3+} in crystals. $S^k = [7/(2k+1)(\begin{smallmatrix}3&3&k\\0&0&0\end{smallmatrix})^2 \Sigma_{q=-k,k}(B_q^k)^2]^{1/2}$.

System	Reference	Site symmetry	N[a]	S^4	S^6
YAG	40	D_2	9	337	207
YVO_4	44	D_{2d}	not stated	184	92
$LaCl_3$	46	C_{3h}	4	38	76
LaF_3	41	C_{2v}	9	123	153
$CsCdBr_3$	45	C_{3v}	6	238	31
$Cs_3Lu_2Br_9$	47	C_{3v}	6	251	44
$Cs_3Lu_2Cl_9$	43	C_{3v}	6	257	48
$Cs_2NaErCl_6$	14	O_h	2	272	61
$Cs_2NaErCl_6$	this study	O_h	2	287	60

[a]Number of crystal field parameters fitted.

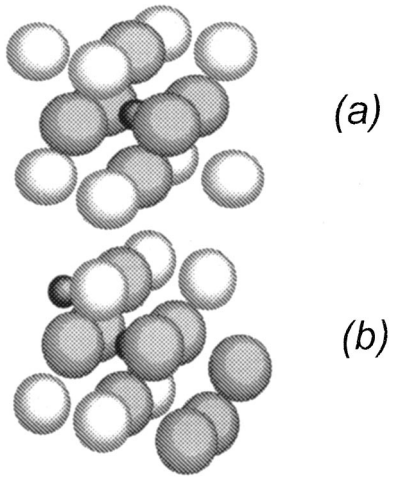

FIG. 6. The rare-earth environment in the (a) $Cs_2NaErCl_6$ and (b) $Cs_3Lu_2Cl_9$ structures. The Er^{3+} (Lu^{3+}), Cl^-, and Cs^+ ions are black, gray, and white, respectively. The threefold axis of $Cs_3Lu_2Cl_9$ is oblique, along the line joining the two lanthanide ions. The fourfold axis of $Cs_2NaErCl_6$ is parallel to the left margin of the page.

away (5.5 Å). Therefore we can visualize the volume which is necessary to build up crystal field parameters: hardly a sphere with a radius equal to 4.0 Å.

V. CONCLUSIONS

Emission has been reported from the $^2I_{11/2}$ term at 40 668 cm^{-1}, with possible ultraviolet laser application in other hosts. This luminescent state is above the previously characterized $^2P_{3/2}$ (Ref. 40) and $^2H(2)_{9/2}$ (Ref. 2) luminescent terms, but below the luminescent $^4D_{1/2}$, $^2F_{7/2}$, and $^2F_{5/2}$ terms.[1] A wealth of transitions have been observed and assigned to the ladder of lower-energy levels. A preliminary investigation of the ultraviolet absorption spectrum of $Cs_2NaErCl_6$ has enabled the assignment to be made of 58 crystal field levels of Er^{3+} in this cubic host, with a further 17 levels tentatively identified. The location of these energy levels has facilitated the assignment of luminescent states in the ultraviolet. Emission has also been reported and interpreted from $^2K_{13/2}$ and $^2H(2)_{9/2}$. The largely vibronic character of many transitions leads to complex and extensive spectral features, by contrast with the spectra of Er^{3+} at noncentrosymmetric sites.

The energy-level fit to 58 levels has given a satisfactory mean deviation, which is slightly improved by an empirical correction. It would be advisable to attempt a treatment of the discrepancies by full configuration interaction as has been done previously with success for U^{4+} $(5f^2)$ in the compound Cs_2UBr_6,[53] and for Pr^{3+} $(4f^2)$ in $Cs_2NaPrCl_6$ crystals.[54] This treatment relies upon the establishment of the formal expressions for all the prominent intraconfigurational interactions affecting the f^{11} configuration, which proves to be a difficult process.

ACKNOWLEDGMENT

P.A.T. acknowledges financial support for this work from the Hong Kong RGC, Grant No. CityU1067/99P.

[1] R. T. Wegh, A. Meijerink, R.-J. Lamminmäki, and J. Hölsä, J. Lumin. **87**, 1002 (2000).
[2] P. A. Tanner, M. Chua, W.-M. Kwok, and D. L. Phillips, Phys. Rev. B **60**, 13 902 (1999).
[3] P. A. Tanner, C. S. K. Mak, W.-M. Kwok, D. L. Phillips, and M. F. Joubert, J. Phys. Chem. B **106**, 3606 (2002).
[4] L. R. Morss, M. Siegel, L. Stinger, and N. Edelstein, Inorg. Chem. **9**, 1771 (1970).
[5] M. J. Weber, Phys. Rev. **156**, 231 (1967).
[6] D. R. Tallant, M. P. Miller, and J. C. Wright, J. Chem. Phys. **65**, 510 (1976).
[7] W. Ryba-Romanowski, Z. Mazurak, and B. Jezowska-Trzebiatowska, J. Lumin. **27**, 177 (1982).
[8] P. A. Tanner, Mol. Phys. **63**, 365 (1988).
[9] W. Ryba-Romanowski, S. Golab, and W. A. Pisarski, J. Phys.: Condens. Matter **7**, 7397 (1995).
[10] Z. Mazurak, E. Lukowiak, B. Jezowska-Trzebiatowska, and W. Ryba-Romanowski, J. Lumin. **29**, 47 (1984).
[11] Z. Mazurak, E. Lukowiak, and B. Jezowska-Trzebiatowska, J. Lumin. **33**, 159 (1985).
[12] M. Campbell and C. D. Flint, Proc. SPIE **3176**, 98 (1997).
[13] M. Campbell, W. Humbs, J. Strasser, H. Yersin, and C. D. Flint, Proc. SPIE **3176**, 103 (1997).
[14] Z. Hasan, L. Biyikli, M. J. Sellars, G. A. Khodaparast, F. S. Richardson, and J. R. Quagliano, Phys. Rev. B **56**, 4518 (1997).
[15] M. Wermuth, A. Schmitz, and H. Güdel, Phys. Rev. B **63**, 245118 (2001).
[16] W. Ryba-Romanowski, G. Dominiak-Dzik, and S. Golab, J. Phys.: Condens. Matter **6**, 1593 (1994).
[17] M. Campbell and C. D. Flint, Spectrochim. Acta, Part A **54**, 1583 (1998).
[18] Z. Hasan and F. S. Richardson, Mol. Phys. **45**, 1299 (1982).
[19] P. A. Tanner, Mol. Phys. **57**, 737 (1986).
[20] B. Jezowska-Trzebiatowska, W. Ryba-Romanowski, Z. Mazurak, and J. Hanuza, Chem. Phys. **50**, 209 (1980).
[21] S. M. Crooks, M. F. Reid, P. A. Tanner, and Y. Y. Zhao, J. Alloys Compd. **250**, 297 (1997).
[22] P. A. Tanner, A. DePiante, F. S. Richardson, and M. F. Reid, Mol. Phys. **60**, 1037 (1987).
[23] P. A. Tanner, V. V. R. K. Kumar, C. K. Jayasankar, and M. F. Reid, J. Alloys Compd. **215**, 349 (1994).
[24] M. R. Roser, J. Xu, S. J. White, and L. R. Corruccini, Phys. Rev. B **45**, 12 337 (1992).
[25] P. A. Tanner, S. Xia, Y. L. Liu, and Y. Ma, Phys. Rev. B **55**, 12 182 (1997).
[26] A. Lentz, J. Phys. Chem. Solids **35**, 827 (1974).
[27] M. P. Hehlen, H. U. Güdel, and J. R. Quagliano, J. Chem. Phys. **101**, 10 303 (1994).
[28] A. DePiante, F. S. Richardson, and Z.-ul Hasan, J. Chem. Phys. **82**, 1102 (1985).
[29] P. A. Tanner, A. DePiante, F. S. Richardson, and M. F. Reid, Mol. Phys. **60**, 1037 (1987).
[30] P. A. Tanner, Chem. Phys. Lett. **145**, 134 (1988).
[31] B. R. Judd, *Operator Techniques in Atomic Spectroscopy*, (Princeton University, Princeton, NJ, 1998).
[32] B. G. Wybourne, *Spectroscopic Properties of Rare Earths* (Wiley, New York, 1965).
[33] B. R. Judd, Phys. Rev. **141**, 141 (1966).
[34] K. Rajnak and B. G. Wybourne, Phys. Rev. **132**, 280 (1963).
[35] M. Faucher and D. Garcia, C. R. Acad. Sci., Ser. I: Math. **307**, 607 (1988).
[36] M. Faucher, D. Garcia, and P. Porcher, C. R. Acad. Sci., Ser. I: Math. **308**, 603 (1989).
[37] C. L. Li and M. F. Reid, Phys. Rev. B **42**, 1903 (1990).
[38] O. K. Moune, D. Garcia, and M. Faucher, J. Phys. Chem. Solids **52**, 513 (1991).
[39] C. W. Nielson and G. F. Koster, *Spectroscopic Coefficients for the p^n, d^n, and f^n Configurations*, (MIT, Cambridge, MA, 1963).
[40] J. B. Gruber, J. R. Quagliano, M. F. Reid, F. S. Richardson, M. E. Hills, M. D. Seltzer, S. B. Stevens, C. A. Morrison, and T. H. Allik, Phys. Rev. B **48**, 15 561 (1993).

[41] W. T. Carnall, G. L. Goodman, K. Rajnak, and R. S. Rana, Argonne National Laboratories Report No. ANL-88-8, 1988 (unpublished).
[42] R. G. Denning, Spectrochim. Acta, Part A **55**, 1757 (1999).
[43] S. R. Lüthi, H. U. Güdel, M. P. Hehlen, and J. R. Quagliano, Phys. Rev. B **57**, 15 229 (1998).
[44] J. A. Capobianco, P. Kabro, F. S. Ermeneux, R. Moncorgé, M. Bettinelli, and E. Cavalli, Chem. Phys. **214**, 329 (1997).
[45] J. R. Quagliano, N. J. Cockroft, K. E. Gunde, and F. S. Richardson, J. Chem. Phys. **105**, 9812 (1996).
[46] K. W. Krämer, H. U. Güdel, and R. W. Schwartz, Phys. Rev. B **56**, 13 830 (1997).
[47] M. P. Hehlen, H. U. Güdel, and J. R. Quagliano, J. Chem. Phys. **101**, 10 303 (1994).
[48] F. Auzel, Mater. Res. Bull. **14**, 223 (1979).
[49] M. Kibler, Phys. Lett. **98A**, 343 (1983).
[50] M. Faucher, D. Garcia, and C. K. Jørgensen, Chem. Phys. Lett. **129**, 387 (1986).
[51] N. L. Chang, J. B. Gruber, R. P. Leavitt, and C. A. Morrison, J. Chem. Phys. **76**, 3877 (1982).
[52] G. Meyer and A. Schönemund, Mater. Res. Bull. **15**, 89 (1980).
[53] M. D. Faucher, O. K. Moune, D. Garcia, and P. Tanner, Phys. Rev. B **53**, 9501 (1996).
[54] P. A. Tanner, C. S. K. Mak, and M. D. Faucher, J. Chem. Phys. **114**, 10 860 (2001).